



ORIGINAL RESEARCH ARTICLE

Wear and Frictional Behavior of Copper Modified Ti-6Al-4V Alloy

G.V.S. Nageswara Rao, Polamuri Sudheer Kumar, and Naga Sruthi Neelam

Submitted: 25 September 2023 / Revised: 24 March 2024 / Accepted: 26 April 2024

The effect of copper addition on the dry sliding wear and frictional behavior of Ti-6Al-4V alloy in different heat treatment conditions, i.e., in $\alpha + \beta$ phase field and β phase field, was investigated using pin-on-disk method. The hardness of the alloy subjected to solution treatment followed by aging, exhibited relatively higher hardness than solution treated alloy due to the precipitation of Ti_2Cu intermetallic. The wear rate, average coefficient of friction and maximum temperature attained during sliding test were determined and reported as a function of varying load of 10-50 N at sliding velocities of 0.25, 1 and 1.5 m/s. The wear rate increased with load, whereas it decreased initially with sliding velocities till 1 m/s and increased beyond that. The average coefficient of friction and maximum temperature were observed to be directly dependent on the load, whereas sliding velocity exhibited a different influence on coefficient of friction. Aging treatment resulted in lower coefficient of friction and maximum temperature attained during the test. The morphological evaluation of wear tracks and wear debris was also carried out and is presented in the current study.

Keywords Cu addition, pin-on-disk method, Ti64, wear

1. Introduction

Ti-6Al-4V (Ti64), an $\alpha + \beta$ titanium alloy, is the most used titanium alloy in aerospace, automobile, marine, medical and chemical industries due to its unique combination of mechanical properties, inherent workability and biocompatibility (Ref 1-3). Despite these significant properties, Ti64 alloy suffers from inferior tribological properties, restraining its applications in automobiles mainly due to failure by galling and unstable friction coefficients (Ref 3, 4). The notoriously poor wear resistance of the alloy can be attributed to (1) its low resistance to plastic shearing which weakens the counteract of the material toward adhesion and delamination that is highly influenced by mechanical properties, (2) low protection by tribo-oxides formed as a result of temperatures induced by friction and can be easily removed by spallation and micro-fragmentation during sliding and (3) embrittlement caused by ingress of atmospheric oxygen (Ref 3, 5, 6). Various approaches including surface modifications (Ref 7-11), adjustment of alloy chemistry and thermal processes (Ref 12-20) with varying success were implemented to improve the wear resistance especially intended in the improvement of the alloy performance in ground vehicle engine applications for fuel efficiency (Ref 21). The presence of

α needles in β matrix resists plastic deformation; however, the higher ductility of β phase results in poor wear resistance (Ref 21, 22).

Li et al. (Ref 23) conducted dry sliding wear tests on Ti64 alloy using a pin-on-disk wear tester using sliding velocities ranging from 0.5 to 4 m/s exploring the role of tribo-oxides and their functions. The study revealed a noticeable variation in the wear rate with changing sliding velocity and distinct transitions in wear mechanisms corresponding to different sliding velocities. At lower speeds, the wear was characterized by a combination of delamination and oxidative wear followed by a gradual transition to delamination wear and finally to oxidative wear with the increase in sliding velocity from 2.5 to 4 m/s.

Sahoo et al. (Ref 24) conducted a comprehensive study on the impact of microstructural variations specifically lamellar, bimodal and equiaxed on the solid particle erosion wear behavior of Ti64 alloy at room temperature. Notably, the lamellar microstructure demonstrated superior erosion resistance compared to bimodal and equiaxed microstructures. The primary mechanism of material loss in the erosion of Ti64 alloy was identified as plowing or pileup, leading to the formation of platelets.

Hadke et al. (Ref 25) delved into the impact of quenching and aging treatment on the microstructure and abrasive wear of Ti64 alloy. The initial alloy underwent solution treatment at 1339 K, followed by oil quenching and subsequent aging at 823 K for 4 h. The as-received specimen exhibited a microstructure consisting of very fine α grains, with an average grain size of 2 μm , and β phase uniformly dispersed throughout. In the quench-aged specimen, the microstructure revealed plates formed by the decomposition of α' during aging. The β phase precipitated out of α' martensite during aging, leading to its uniform dispersion in the α matrix. Two-body abrasive wear tests were conducted on both the as-received and quench-aged specimens using a pin-on-disk apparatus with SiC as the abrasive media. Surprisingly, the wear resistance of the as-

G.V.S. Nageswara Rao, Department of Metallurgical and Materials Engineering, National Institute of Technology Warangal, Hanamkonda 506004, India; Polamuri Sudheer Kumar, Department of Mechanical Engineering, Indian Institute of Technology Tirupati, Tirupati 517506, India; and Naga Sruthi Neelam, Department of Metallurgical and Materials Engineering, National Institute of Technology Raipur, Raipur 492010, India. Contact e-mail: nsneelam.mme@nitrr.ac.in.

received specimen surpassed that of the quench-aged specimen, despite the latter exhibiting higher hardness.

Enhancing wear resistance in materials involves various approaches, such as surface modification, adjustments in alloy chemistry and heat treatment. A relatively unexplored avenue in titanium alloy development is the application of strengthen-

Table 1 Details of raw material used for the melting of Ti-6Al-4V-2.5Cu alloy (for 420 g weight pancake)

Material	Weight, g
Ti sponge chips	367.5
Al chips	22.35
Al-V master alloy (14.5% Al + 85.5%V)	19.65
Cu chips (pure)	10.50

Table 2 Details of heat treatments given to Ti-6Al-4V-2.5Cu alloy and corresponding coding

Heat treatment given	Code
$\alpha + \beta$ solution treatment at 900 °C/4 h/WQ	TC900ST
$\alpha + \beta$ solution treatment at 900 °C/4 h/WQ + aging at 500 °C/4 h/AC	TC900STA
β solution treatment at 1010 °C/2 h/WQ	TC1010ST
β solution treatment at 1010 °C/2 h/WQ + aging at 500 °C/4 h/AC	TC1010STA

WQ, Water quenching; AC, Air cooling.

ing through precipitation hardening. An illustrative instance of precipitation strengthening in titanium alloys is the introduction of silicon into the alloy which enhances the creep resistance of titanium alloys by facilitating the precipitation of titanium silicides (Ref 26). Another system demonstrating precipitation strengthening is Ti-Cu, wherein the beta phase has a restricted solubility range for copper. Consequently, the incorporation of copper into titanium alloys provides the opportunity to tailor mechanical properties through age hardening. This advanta-

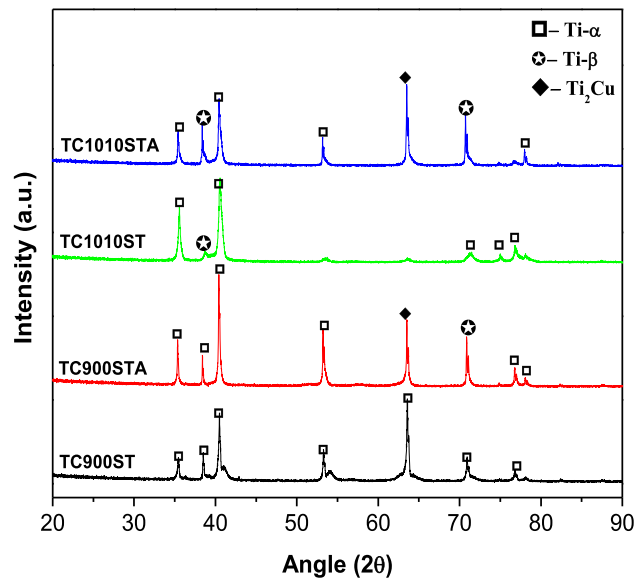


Fig. 2 XRD patterns of the Ti-6Al-4V-2.5Cu alloy in different heat treatment conditions

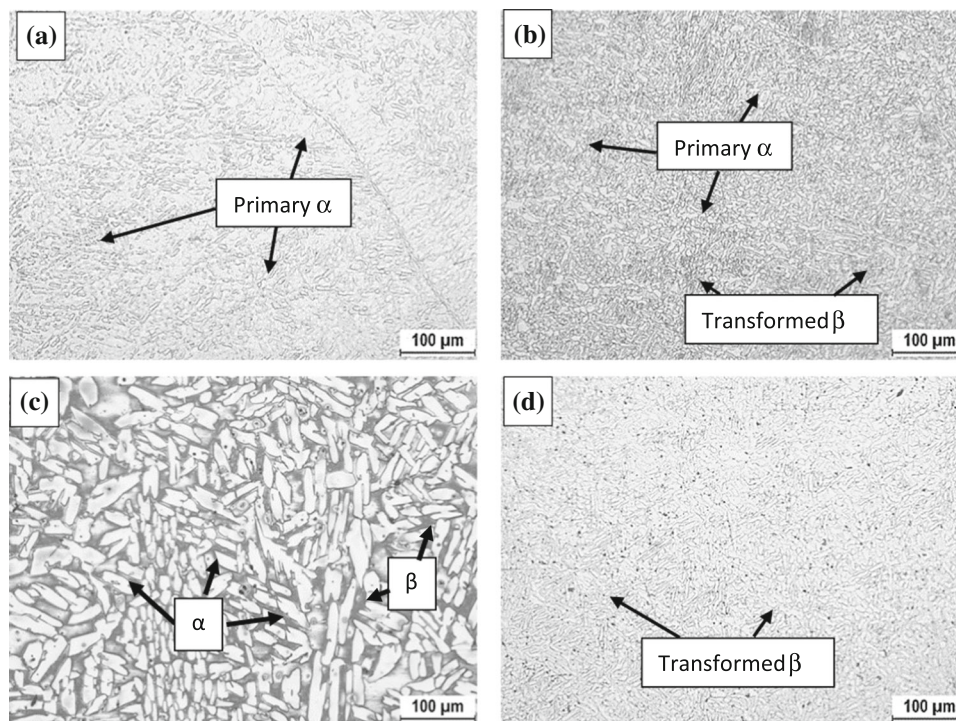


Fig. 1 Optical microstructures of Ti-6Al-4V-2.5Cu alloy in different heat treatment conditions. (a) TC900ST, (b) TC900STA, (c) TC1010ST and (d) TC1010STA

geous aspect of precipitation strengthening has been effectively employed in alloys such as Ti-2.5Cu (Ref 27) and Ti-6Al-1.5V-2.5Cu (Ref 28). Nevertheless, in the case of Ti-6Al-1.5V-2.5Cu, the enhancement in properties compared to Ti-6Al-4V alloy was noted to be marginal. This was ascribed to the variation in vanadium content (copper addition at the cost of vanadium).

The present study aims to investigate the impact of adding 2.5 wt.% of Cu to Ti64, and the influence of four distinct heat treatments ($\alpha + \beta$ solution treatment (TC900ST), $\alpha + \beta$ solution treatment followed by aging (TC900STA), β solution treatment (TC1010ST) and β solution treatment followed by aging (TC1010STA)) on wear and friction behavior under dry sliding conditions at various sliding velocities and loading conditions in terms of wear rate, coefficient of friction and temperature attained during testing has been reported. The study helps in understanding the effect of copper addition on the strength and wear resistance of Ti64 alloy, which can contribute in widening the application window of the alloy.

2. Experimental Details

The Ti-6Al-4V-2.5Cu alloy pancakes were melted in vacuum arc melting furnace (make: Vacuum technologies,

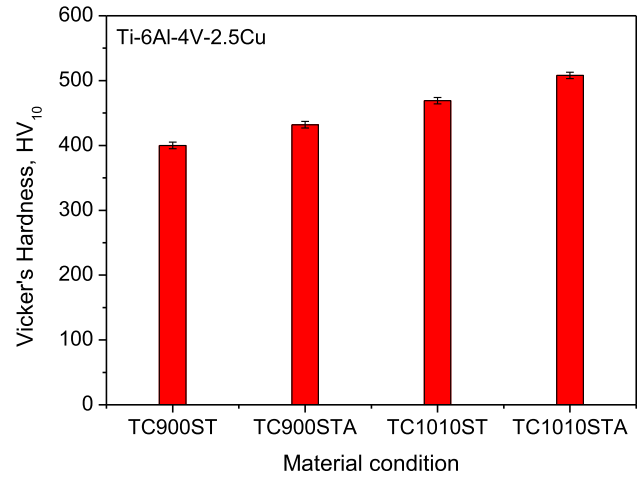


Fig. 4 Vickers hardness of the Ti-6Al-4V-2.5Cu alloy in different heat treatment conditions

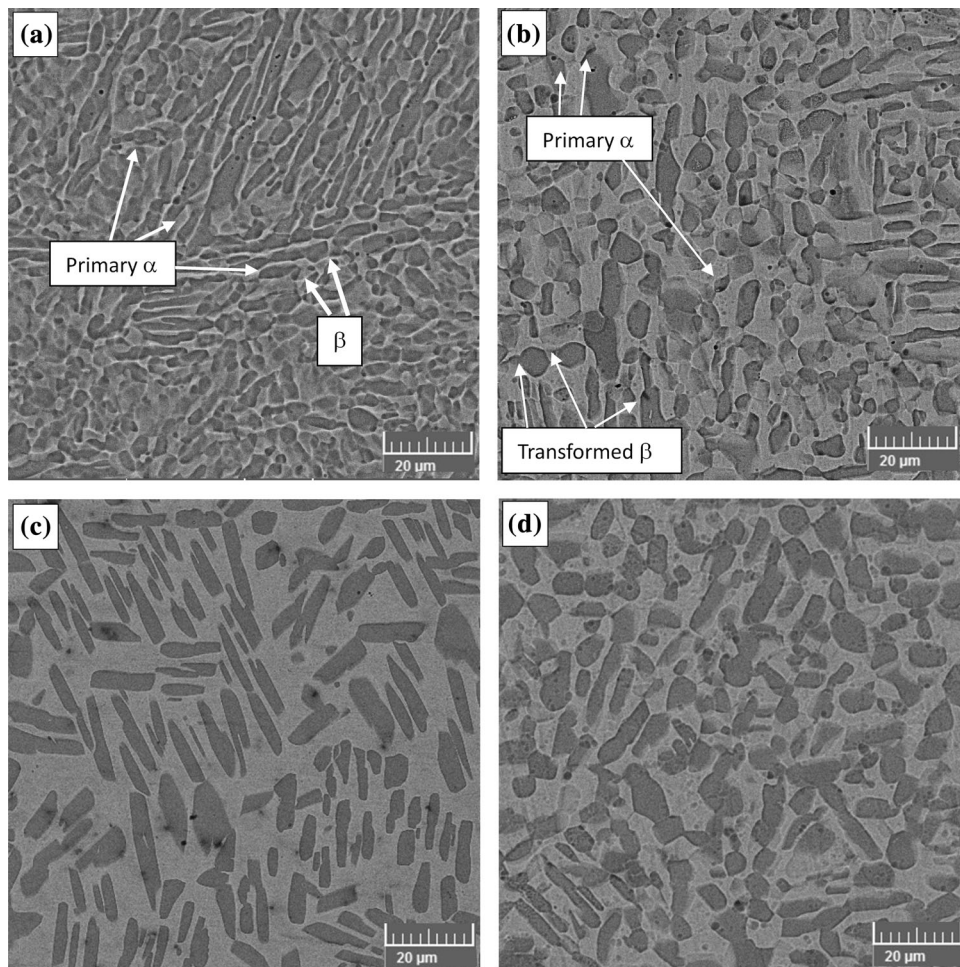


Fig. 3 BSE-SEM images of Ti-6Al-4V-2.5Cu alloy in different heat treatment conditions. (a) TC900ST, (b) TC900STA, (c) TC1010ST and (d) TC1010STA

Bangalore, India). Ti sponge (99.99%), Al and Cu chips, Al-V master alloy were used for melting. The details of raw materials used for melting of 420 g pancake are shown in Table 1. The pancakes were subjected to standard thermomechanical treatments followed by forging (pneumatic hammer (MASSEY)) at 1050 °C in β phase region to break the dendritic structure formed in casting. The thickness was reduced from 11 to 7 mm imparting 40% deformation. To refine the lamellar structure obtained during forging and to get a bimodal $\alpha + \beta$ structure, rolling was performed at 850 °C ($\alpha + \beta$ field) to a thickness of 5 mm followed by subsequent heat treatments. Solution treatment was carried out at two different temperatures, viz. at 900 °C ($\alpha + \beta$ phase region) and at 1010 °C (β phase region) for 2 h and 4 h, respectively, followed by water quenching (WQ). Some plates were subjected to aging at 500 °C for 4 h followed by air cooling (AC) after solutionizing. R-type thermocouple (Platinum-13% Rhodium) was used to monitor the temperature of the samples during heat treatment. To prevent oxidation of the samples during heat treatment, the samples were coated with Henkel made Deltaglaze FB 412[®] colloidal glass solution. The details of different heat treatments that were employed and corresponding coding of the samples are presented in Table 2.

Optical microscope of Leica make (Model: DMi8A) equipped with image analysis was used for microstructural observations. Macrohardness tests were carried out using Matsuzawa make Vickers hardness tester (Model: VMT-X7), with maximum load of 30 kg. The hardness tests were performed using 10 kg load and 15 s dwell time with at least

10 measurements for each sample, and the average with standard deviation was reported.

The dry sliding wear tests were carried out using pin-on-disk wear testing machine (Make: DUCOM and Model: TR-20LE) in air at room temperature (26 ± 2 °C) using hardened EN-31 steel disk (180 mm diameter and 8 mm thick, 63-65 Rc hardness) as counter face material. The pins (4 mm \times 4 mm and 30 mm height) of Ti-6Al-4V-2.5Cu alloy were prepared using wire-cut EDM. The contact surfaces of pins and disk were prepared on 1200 grit SiC paper keeping surface roughness (R_a) in 0.8-2.0 μ m range, degreased, cleaned with acetone and dried prior to each test. The wear tests were carried out at different normal loads (10-50 N) and sliding speeds (0.25-1.5 m/s) for a total sliding distance of 500 m. The rpm of the disk, wear track diameter and sliding time were adjusted to attain a constant sliding distance of 500 m in all the tests. To determine the wear rate, pin initial and final weight were measured using a 0.01 mg precision balance to record the weight loss. Wear rate (mm^3/m) calculations were carried out by dividing volume loss (mm^3) with total sliding distance (m). During each test, the wear and frictional force (from which coefficient of friction (COF) was also determined) were monitored on the computer and the temperature rise at disk-pin contact surface was monitored and recorded by using K-type thermocouple to know the maximum temperature attained during each test. The morphological analysis of the worn surface of the pin and debris was observed by a scanning electron microscope (SEM) of TESCAN make (Model: VEGA3 LMU). The phase analysis of wear debris was done by using x-ray diffraction (XRD) of PANalytical make (Model: X'PERT Powder).

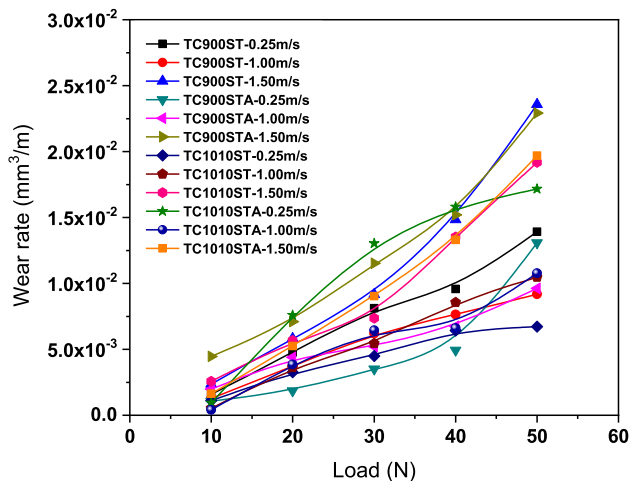


Fig. 5 Comparison of wear rates of the Ti-6Al-4V-2.5Cu alloy as a function of applied load in different heat treatment conditions for different sliding velocities

3. Results and Discussion

3.1 Microstructure and Phase Evaluation

Figure 1(a), (b), (c), and (d) shows the optical images of TC900ST, TC900STA, TC1010ST and TC1010STA alloys, respectively. Primary α (hcp) grains with β phase (bcc) at grain boundaries are seen in TC900ST alloy (Fig. 1a). Upon subsequent aging treatment, TC900STA has revealed primary α grains in aged transformed β matrix (Fig. 1b). Hot working below the β -transus temperature ($\alpha + \beta$ phase region) results in the nucleation and growth of primary α . The morphology is determined by the extent of hot working, varying from elongated plates at about < 30% reduction to equiaxed grains at > 30% reduction (Ref 1, 2). Solution treatment at 900 °C resulted in equiaxed primary α (Fig. 1a) as the reduction in thickness is about 50%. Subsequent aging at 500 °C has resulted in transformed β structure.

Table 3 Sliding velocities at which minimum and maximum wear rate occurs in Ti-6Al-4V-2.5 Cu alloy for different heat treatment conditions

Sample	Sliding velocity at which minimum wear rate occurs, m/s	Sliding velocity at which maximum wear rate occurs, m/s
TC900ST	1	1.5
TC900STA	0.25	1.5
TC1010ST	0.25	1.5
TC1010STA	1	1.5

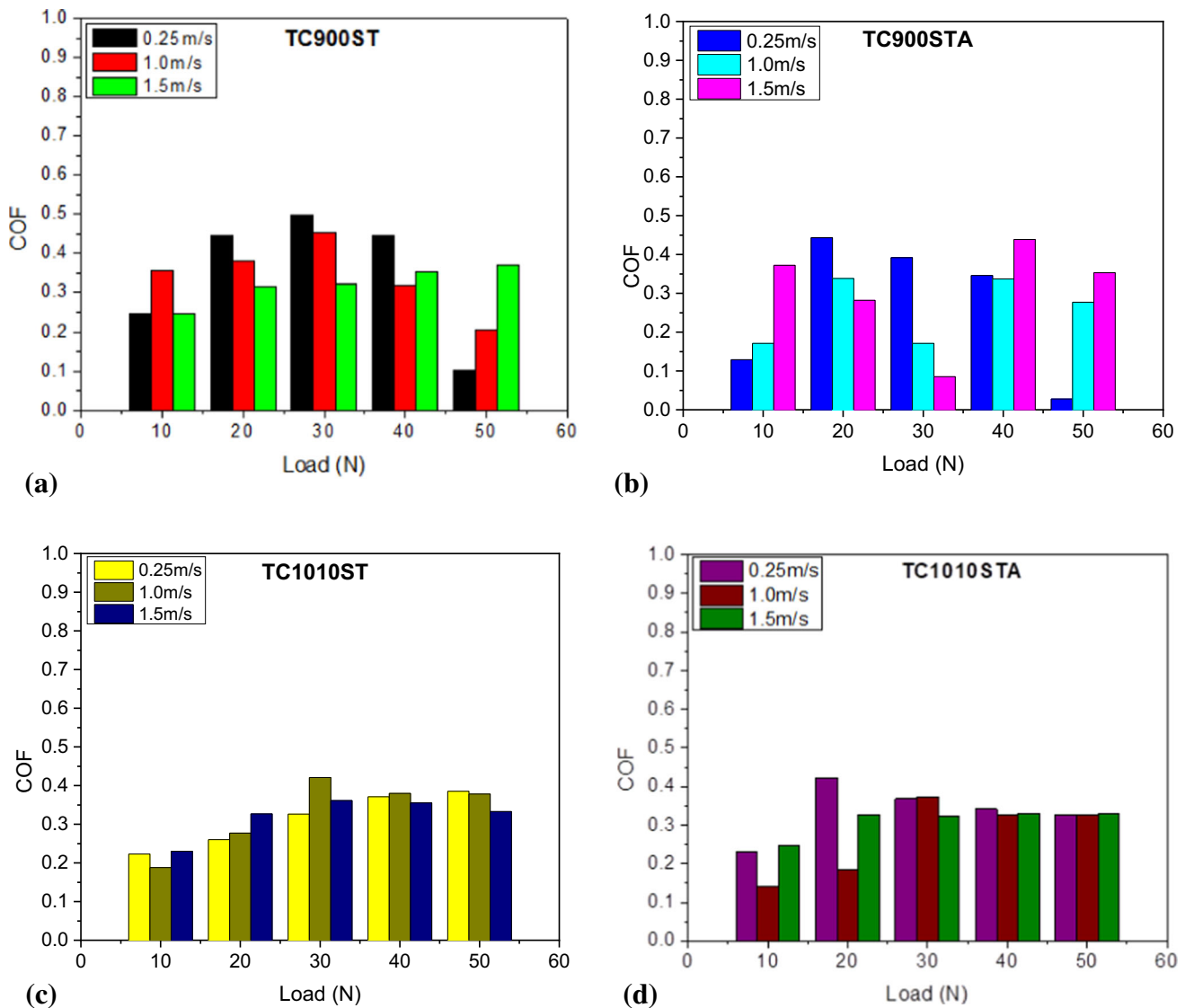


Fig. 6 Coefficient of friction of the Ti-6Al-4V-2.5Cu alloy as function of applied load at different sliding velocities in different heat treatment conditions. (a) TC900ST, (b) TC900STA, (c) TC1010ST and (d) TC1010STA

Figure 1(c) shows the optical microstructure of the TC1010ST alloy (solution treated in β phase field (i.e., 1010 °C/2 h/WQ)). The microstructure consisted of coarse α phase (hcp) lamellae and retained β phase (bcc). As the solvus temperature of Cu in β titanium is significantly lower than the solution treated temperature (i.e., 1010 °C), dissolution of Cu is complete assuming that no phase boundary shift occurs due to ternary additions. Consequent water quenching leads to super saturation of Cu in α martensite due to less time provided for Cu diffusion resulting in primary α and $\alpha' + \beta$, while aging at 500 °C has resulted in transformed β (Fig. 1d).

The presence of α -titanium with minor amount of β in the alloys was confirmed from the XRD measurements (Fig. 2). The precipitation of Ti_2Cu intermetallic is confirmed in TC900STA and TC1010STA after aging. Formation of Ti_2Cu precipitates in Ti-Cu alloys was reported earlier as well (Ref 29-31). Figure 3 shows the SEM images of the alloys strongly supporting the above observations. However, the fine Ti_2Cu precipitates are not revealed in optical and SEM micrographs due to resolution limit.

3.2 Hardness

Figure 4 shows the Vickers hardness values of the alloy in various heat-treated conditions. All the samples irrespective of heat treatment exhibited higher hardness when compared to conventional Ti64 alloy (~ 300HV) (Ref 1, 2, 30). Hardness of β phase region treated alloys (solution treatment at 1010 °C) (TC1010ST) is superior to that of $\alpha + \beta$ phase field treated alloy (solution treatment at 900 °C) (TC900ST) which can be accredited to the transformed β structure in TC1010ST condition (Ref 29, 30). Furthermore, aged alloys (TC900STA and TC1010STA) exhibited significantly higher hardness than un-aged alloys (TC900ST and TC1010ST) of which TC1010STA demonstrates highest hardness due to the formation of Ti_2Cu intermetallic precipitates (Fig. 2).

3.3 Wear Behavior

3.3.1 Effect of Load and Sliding Velocity On. 3.3.1.1 Wear Rate.

Figure 5 shows the effect of load (10-50 N) and

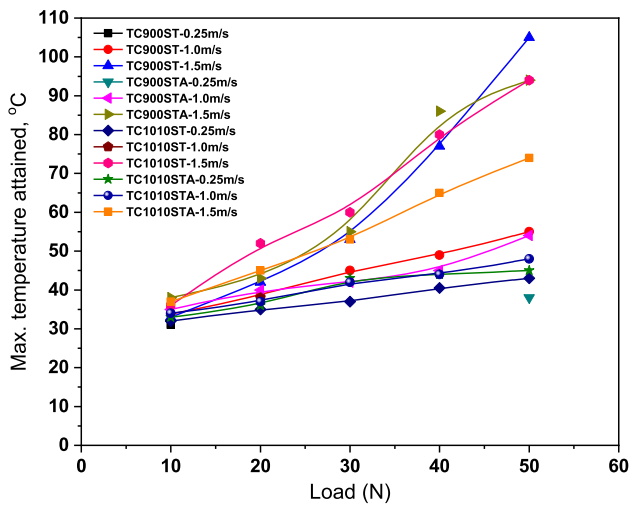


Fig. 7 Comparison of maximum temperatures attained during sliding of the Ti-6Al-4V-2.5Cu alloy as function of sliding velocity at different loads in different heat treatment conditions

sliding velocities (0.25-1.5 m/s) on the wear rate of the alloy in different heat-treated conditions, respectively. It can be observed that in all the heat-treated conditions wear rate increases with the increase in normal load (Fig. 5). However, the wear rate changes with the change in sliding velocity for various heat-treated conditions. The velocities at which the minimum and maximum wear rates occur are presented in Table 3. It can be noted that the alloy exhibits maximum wear rate at a sliding velocity of 1.5 m/s in all heat-treated conditions, whereas minimum wear rate at 1 m/s, except in few cases.

Across all heat-treated conditions, the wear rate shows minimal variation, particularly at sliding velocities ranging from 0.25 to 1.5 m/s and under loading conditions of 10 to ~ 20 N. However, the wear rate exhibits maximum variation at the loading condition of 50 N for varying sliding velocities, as shown in Fig. 5(a), (b), (c) and (d). Notably, the wear rate remains relatively stable and lower at a sliding velocity of 1.0 m/s up to ~ 30 N loading range. A consistent trend in wear rate is observed in both TC900ST and TC900STA conditions,

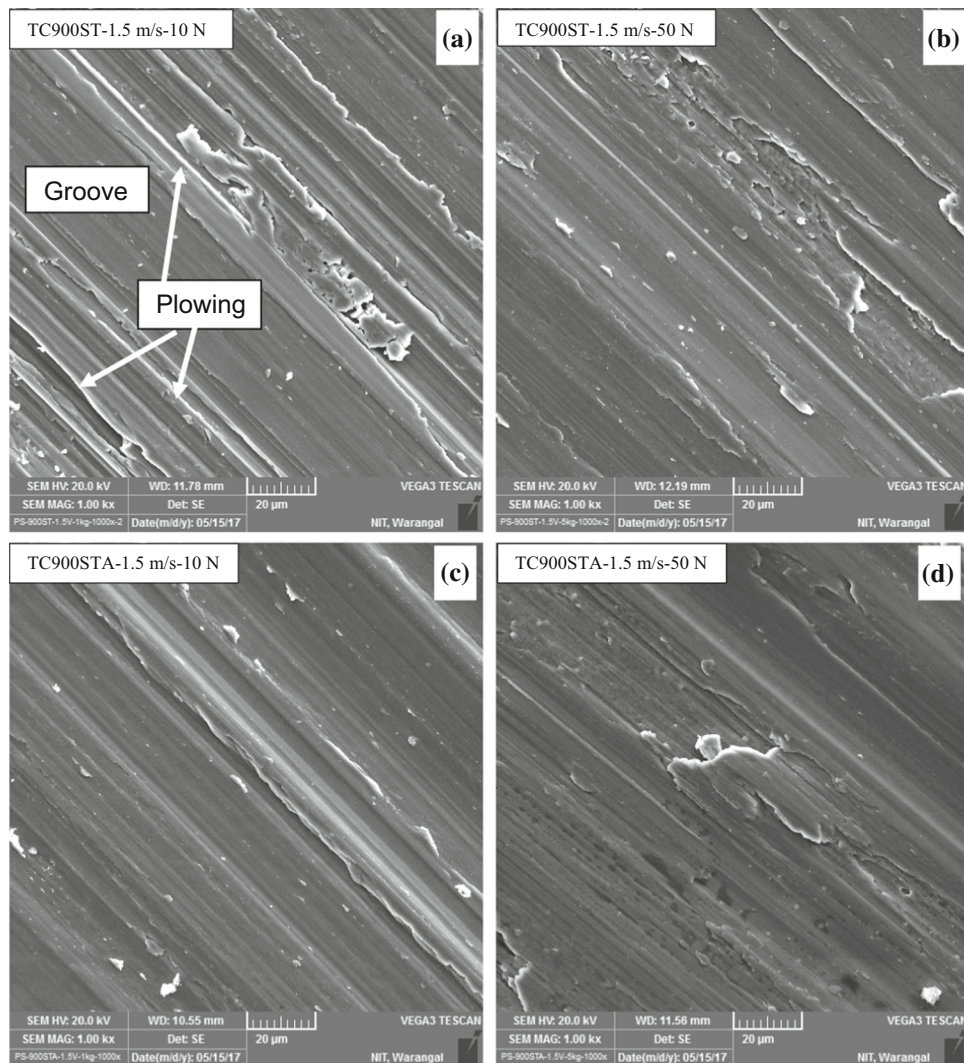


Fig. 8 SEM micrographs of the wear tracks obtained on (a & b) TC900ST and (c & d) TC900STA alloy pins tested at 10 N (left) and 50 N (right) loads at a different sliding velocity 1.5 m/s

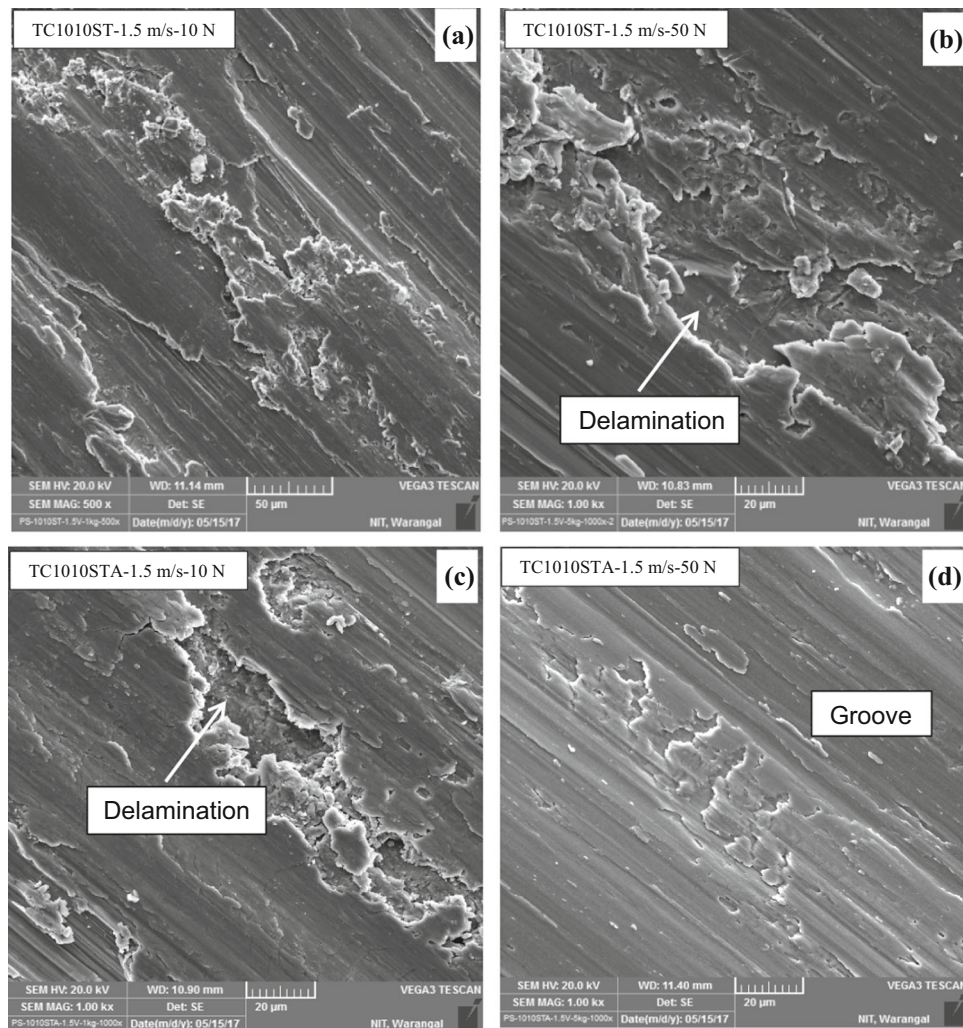


Fig. 9 SEM micrographs of the wear tracks obtained on (a & b) TC1010ST and (c & d) TC1010STA alloy pins tested at 10 N (left) and 50 N (right) loads at a different sliding velocity 1.5 m/s

as depicted in Fig. 5(a) and (b). Conversely, some variation in wear rate is observed in TC1010ST and TC1010STA conditions, as shown in Fig. 5(c) and (d). However, it is noteworthy that, regardless of the heat-treated conditions, the wear rate tends to be higher at a combination of sliding velocity of 1.5 m/s and a load of 50 N. The increase in wear with the increase in sliding speed indicates the delamination mechanism which is attributed to the thermal softening occurring in the material during wear (Ref 32).

3.3.1.2 Coefficient of Friction (COF). The coefficient of friction varied differently in different heat-treated conditions at different loads and sliding velocities (Fig. 6a–d). Aged samples show low coefficient of friction compared to un-aged ones. Further, the combination of low sliding velocity and lower normal load resulted in low coefficient of friction. Among all the heat-treated conditions, the COF exhibits minimal variation concerning load and sliding velocity, especially in the TC1010ST and TC1010STA conditions, as depicted in Fig. 6(c) and (d).

3.3.1.3 Maximum Temperature Attained during Test. It can be observed that the temperature at the pin–disk contact area increases with the increase in load and sliding velocity (Fig. 7). The maximum temperature attained during sliding is low at

lower load (10N) and lower sliding velocities (0.25 m/s) and higher at the higher load and higher sliding velocities (50N and 1.5 m/s), respectively. The alloy subjected to aging treatment (TC900STA and TC1010STA) experienced lower maximum temperatures than those in solution-treated condition (TC900ST and TC1010ST). The maximum temperatures attained during the sliding test range from 30–38 °C at 10 N and 38–104 °C at 50 N loads. From the results, it can be concluded that aging treatment has reduced the tendency to raise the temperature of the alloy during sliding.

3.3.2 Worn Surface Analysis. The SEM micrographs of the worn surface of the alloy pins in different heat-treated conditions are shown in Fig. 8 and 9. The alloy in all heat-treated conditions exhibited sliding marks characterized with grooves and ridges illustrating smearing, plowing and plastic deformation. However, plastic deformation is not so considerable at low loads and sliding velocities. Flake-like metallic debris are generated at high loads and sliding velocities. The presence of continuous grooves and micro-cuttings on the wear tracks indicates abrasion. In the cases of metal-on-metal sliding contact situation, the possibility of two-body abrasion can be expected due to plowing action of sharp asperities present on a

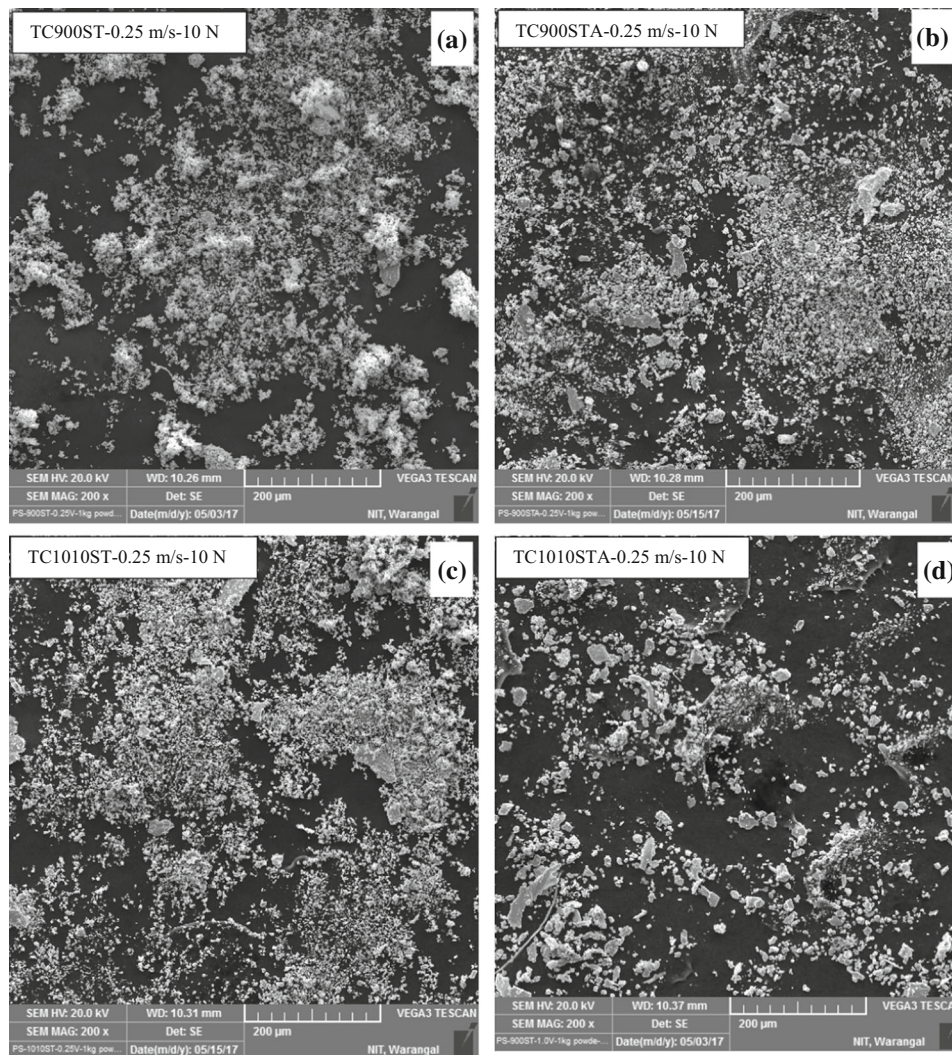


Fig. 10 SEM micrographs of the wear debris of (a & b) TC900ST and TC900STA; (c & d) of TC1010ST and TC1010STA alloy pins tested at 10 N at sliding velocity 0.25 m/s

hard surface (in the present case En-31 steel disk, hardness $\approx 63\text{-}65$ HRc $\approx 780\text{-}840$ HV₁₀). At the onset of wear, the hard asperities penetrate the softer surface (in the present case Ti-6Al-4V-2.5Cu alloy pins, hardness $\approx < 510$ HV₁₀) under the normal contact pressure. When a lateral motion is executed, removal of material from the softer surface due to collective effects of 'micro-plowing,' 'micro-cutting' and 'micro-cracking' occurs, resulting in grooves and scratches on the worn surface as shown in Fig. 8 and 9. The shifting of materials toward the groove sides occurs when the pin plows into the disk surface and this is known as plowing mechanism which is evident from the distinct parallel furrows in the sliding direction on the wear track. The wear debris often takes micro-cutting chips form.

At low load (10 N) and low sliding velocity (0.25 m/s), the alloy exhibited the ductile, plowing type of metallic wear in all heat treatment conditions. The wear tracks are clear, smooth and formed uniform grooves with less plastic deformation. The worn surface of TC900ST (0.25 m/s at 10 N) pins exhibited less plastic deformation due to the formation of oxide scale reducing the interaction between the disk and pin.

The wear track indicates a micro-fragmentation process. Smooth compacted layers in the direction of sliding were

observed in the specimens tested at 0.25 m/s, whereas plastically deformed layers in the case of 1 m/s and 1.5 m/s. Many abrasive grooves under the smooth layers were detected in the direction of sliding. Abrasive action of the hard carbides in the steel disk can be attributed for these grooves (Ref 33, 34).

At high load (50 N) and high velocity (1.5 m/s) (Fig. 8b), brittle detachment of large particles from the surface forming non-uniform grooves is clearly seen. At intermediate loads and intermediate velocity, combined features of low and high conditions can be observed. In TC900STA (Fig. 8c) and TC1010STA (Fig. 9c) condition, the plowed surface exhibited perpendicular cracks which are result of subsurface cracks propagation to the worn surface as the deformation progresses (Ref 33, 34). Along with these cracks, galling wear appearance suggesting delamination is also observed in the SEM images of TC1010ST and TC1010STA (Fig. 8 and 9) indicating adhesive wear. Therefore, it is believed that higher wear rate is a resultant of abrasive wear and delamination of the deformed surface layers.

3.3.3 Wear Debris Analysis. 3.3.3.1 Morphological Analysis.

The debris collected from wear tests of TC900ST,

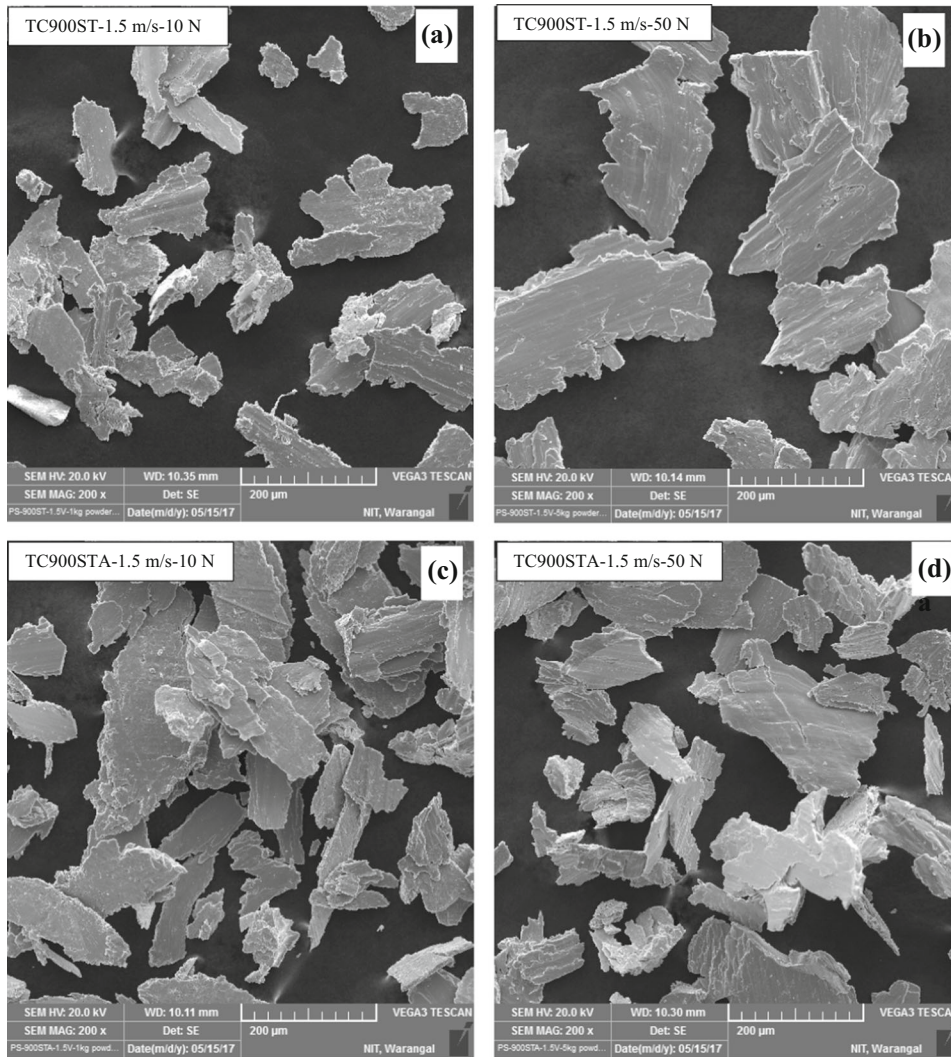


Fig. 11 SEM micrographs of the wear debris of (a & b) TC900ST and (c & d) of TC900STA alloy pins tested at 10 N (left) and 50 N (right) loads at sliding velocity 1.5 m/s

TC900STA, TC1010ST and TC1010STA at different loads (10 and 50 N) and sliding velocities (0.25, 1, 1.5 m/s) were analyzed to determine the wear mechanism, and few are shown in Fig. 10, 11, and 12. The general trend of the morphology of wear debris is as follows: At low loads (10 N) and low sliding velocity, the wear debris are fine (ranging between 1 and 5 μm) and only some flake-like debris (about 20-30 μm width) are intermittently present. However, at high loads (50 N) and high sliding velocity (1.5 m/s) the wear debris are in the form of large flakes/chips (average length of > 200-250 μm , width of 50-100 μm). The mixed morphologies of the debris at intermediate velocities indicate that large flake-type debris increases with the increase in sliding velocity.

The loose and fine debris observed at low loads and sliding velocities indicates micro-fragmentation process, which is apparent in oxidative wear, while chip-like debris indicates micro-cutting action during wear (Ref 34, 35). Hence, at low load and sliding velocity abrasive wear occurs, whereas large amount of flake-like wear debris (plate-like particles), an indicative of delamination wear, occurs at high load and sliding velocity combination (Ref 33, 34). In addition, the large flake-like debris (length: 200-250 μm and width: 100-150 μm)

indicates that the sliding wear is more rigorous at higher loads (50 N) and velocities (1.5 m/s). Figure 10, 11, and 12 suggests that the size of the flake-like debris is increased with increasing the load and sliding velocity and these are formed due to severe plastic deformation. At low load and sliding velocities, influence of metallic wear is insignificant; nevertheless, it becomes significant with increasing load and velocities as indicated by the increased presence of plate-like debris (Ref 36-38).

At lower linear speed (e.g., 0.3 m/s) Molinari et al. (Ref 35) mainly observed the oxidative wear, whereas with the increase in linear speed, at 0.8 m/s, only delamination wear mechanism was found in Ti-6Al-4V. Although much higher speed (1.5 m/s) is employed in the current study, the delamination wear identified in the alloy agrees with the work of Molinari et al. (Ref 35). One of the reasons for poor tribological properties of pure Ti and Ti64 can be ascribed to their incapability of forming a protective oxide layer during wear (Ref 35), and no such protective oxidation constituents were detected in the current study as well. Based on these observations, severe delamination wear is suggested as the wear mechanism in the current experimental conditions in Ti-6Al-4V-2.5Cu alloy.

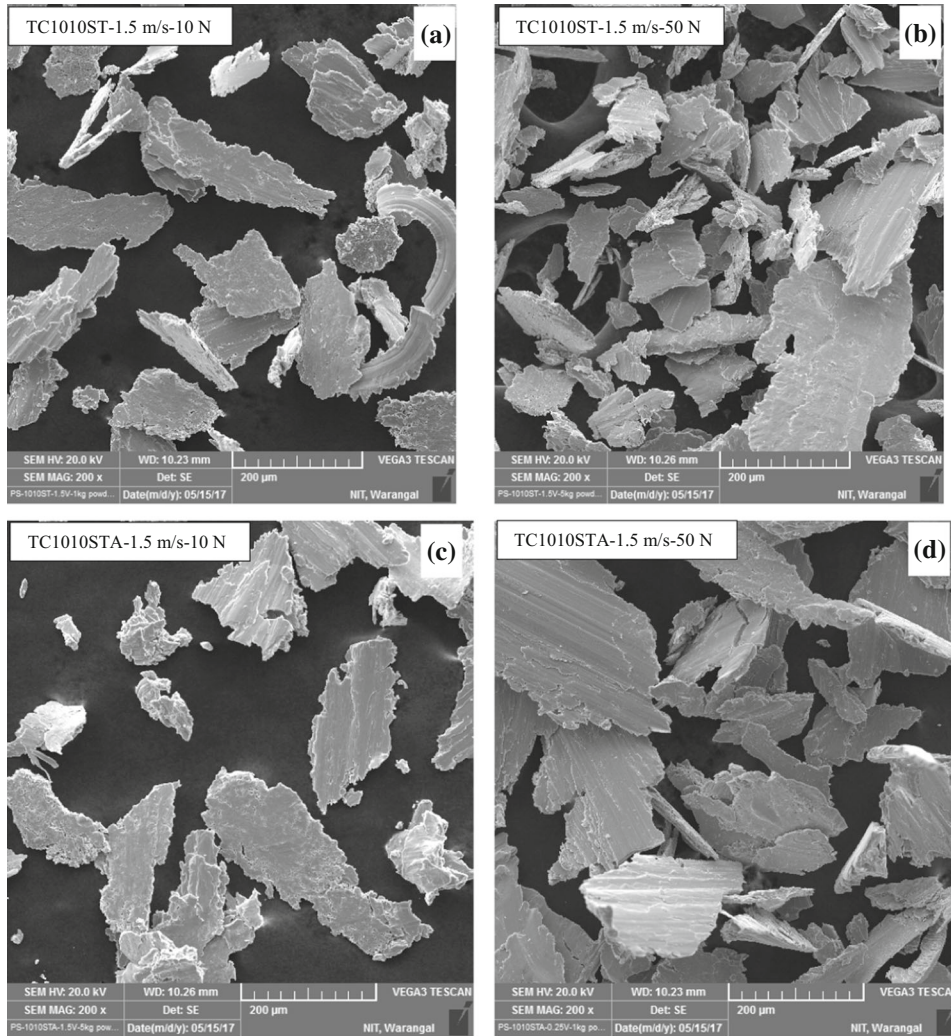


Fig. 12 SEM micrographs of the wear debris of (a & b) TC1010ST and (c & d) TC1010STA alloy pins tested at 10 N (left) and 50 N (right) loads at sliding velocity 1.5 m/s

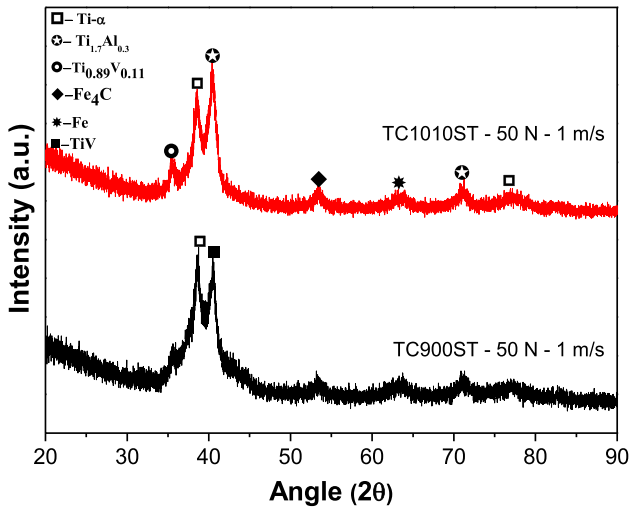


Fig. 13 XRD spectra of wear debris collected at 50 N load and 1 m/s sliding velocity

3.3.3.2 Phase Analysis by XRD. The metallic debris of TC900ST and TC101ST obtained at 50 N load and 1 m/s sliding velocity were analyzed (Fig. 13). In case of TC900ST, the debris comprises α -Ti and TiV, whereas in the case of TC1010ST, α -Ti and Ti-Al and Ti-V intermetallics. The weak reflections corresponding to Fe, and Fe_4C probably resulted from the wear of disk material. The plate-like debris in Fig. 11 and 12 are composed of α -Ti. Molinari et al. (Ref 35) reported that at the lowest sliding velocity, the major portion of debris is constituted by a mixture of TiO and metallic α -Ti. On the other hand, with the increase in sliding speed, metallic α -Ti ratio increases with minor fractions of compacted TiO particles. The presence of α -Ti agrees with Molinari et al. (Ref 35) confirming the metallic nature of plate-like debris.

4. Conclusions

- XRD studies of Ti-6Al-4V-2.5Cu revealed Ti_2Cu precipitates after aging.

- The alloy in all heat-treated conditions exhibited higher hardness than that of conventional Ti64 alloy.
- The hardness of TC1010ST and TC1010STA is higher than that of TC900ST and TC900STA alloys. The increase in hardness is observed upon aging. This is due to the formation of Ti₂Cu precipitates in the aged sample.
- There is an increase in wear rate of the alloy in both ST and STA conditions upon increasing the load. At lower loads and sliding velocities, the alloy in all heat-treated conditions exhibits lower wear rate due to oxidation wear, whereas at higher loads and sliding velocities wear rate is more in all heat-treated and aged conditions due to delamination wear.
- Higher wear rate is mainly due to the inability of Ti-6Al-4V-2.5Cu alloy to form oxide (protective) layer.
- At lower loads and lower sliding velocities, the worn-out metal debris is fine in size, while at higher loads and higher sliding velocities debris are of flake-like morphology.
- Severe delamination wear is the proposed wear mechanism in the current experimental conditions in Ti-6Al-4V-2.5Cu alloy.

Acknowledgments

The authors gratefully acknowledge Dr. Amit Bhattacharjee, Titanium alloy Group, DMRL, Hyderabad, for proving the Ti-6Al-4V-2.5Cu alloy for this work. The authors also thank the Director, NIT Warangal, for continuous support.

References

1. G. Lutjering and J.C. Williams, *Titanium*, Springer, Berlin, Heidelberg, 2007
2. M. Peter and C. Leyens, *Titanium and Titanium Alloys*, Wiley VCH, 2003
3. K.G. Budinski, Tribological Properties of Titanium Alloys, *Wear*, 1991, **151**, p 203–217.
4. G.D. Revankar, R. Shetty, S.S. Rao, and V.N. Gaitonde, Wear Resistance Enhancement of Titanium Alloy (Ti-6Al-4V) by Ball Burnishing Process, *J. Mater. Res. Technol.*, 2017, **6**(1), p 13–32.
5. X.H. Cui, Y.S. Mao, M.X. Wei, and S.Q. Wang, Wear Characteristics of Ti-6Al-4V Alloy at 20–400 °C, *Tribol. Trans.*, 2012, **55**, p 185–190.
6. S. Yerramareddy and S. Bahadur, The Effect of Laser Surface Treatments on the Tribological Behavior of Ti-6Al-4V, *Wear*, 1992, **157**, p 245–262.
7. G. Manisavagam, K.S. Amritpreet, A. Rajamanickam, and K.G. Ashok, Ti Based Biomaterials: The Ultimate Choice for Orthopedic Implants: A Review, *Prog. Mater. Sci.*, 2009, **54**(3), p 397–425.
8. R. Johnson, J. Eberhardt, Thermal Oxidation: A Promising Surface Treatment for Titanium Engine Parts, Transportation Program Oak Ridge National Laboratory, 2006
9. L. Xuanyong, K.C. Paul, and D. Chuanxian, Surface Modification of Titanium, Titanium Alloys and Related Materials for Biomedical Application, *Mater. Sci. Eng. R*, 2004, **47**, p 49–121.
10. H. Guleryuz and H. Cimenoglu, Surface Modification of a Ti-6Al-4V Alloy by Thermal Oxidation, *Surf. Coat. Technol.*, 2005, **192**, p 164–170.
11. F. Borgioli, T.E. Galvanetto, F. Lozzelli, and G. Pradelli, Improvement of Wear Resistance of Ti-6Al-4V Alloy by Means of Thermal Oxidation, *Mater. Lett.*, 2005, **59**, p 2159–2162.
12. S.C. Mishra, B.B. Nayak, B.C. Mohanty, and B. Mills, Surface Nitriding of Titanium in Arc Plasma, *J. Mater. Process. Technol.*, 2003, **132**, p 143–148.
13. Y. Luo, S. Ge, H. Liu, and Z. Jin, Microstructure Analysis and Wear Behavior of Titanium Cermet Femoral Head with Hard TiC Layer, *J. Biomech.*, 2009, **42**, p 2708–2711.
14. G. Kartal, S. Timur, M. Urgen, and A. Erdemir, Electrochemical Boriding of Titanium for Improved Mechanical Properties, *Surf. Coat. Technol.*, 2010, **204**, p 3935–3939.
15. C. Alves Jr., C. Guerra Neto, G. Morais, C. Silva, and V. da Hajek, Nitriding of Titanium Disks and Industrial Dental Implants Using Hollow Cathode Discharge, *Surf. Coat. Technol.*, 2005, **194**, p 196–202.
16. F. David, N. Liam, B. Greg, B. Nicholas, and P.D. Denis, Wear Resistance Enhancement of the Titanium Alloy Ti-6Al-4V via Novel Co-incident Micro Blasting Process, *Surf. Coat. Technol.*, 2011, **205**, p 4941–4947.
17. B.K.C. Ganesh, W. Sha, N. Ramanaiah, and A. Krishnaiah, An Effect of Shot Peening on Sliding Wear and Tensile Behavior of Titanium Implant Alloys, *Mater. Des.*, 2014, **56**, p 480–486.
18. N.S.M. El-Tayeb, *Frictional Behaviour of Burnished Copper Surfaces under Dry Contact Conditions*, Engineering Research Bulletin, HU, Cairo, 1994, p 171–184
19. N.S.M. El-Tayeb, M.I. Ghobrial, The Mechanical Wear Behavior of Burnishing Surfaces. *Proceedings 4th International Conference on Production Engineering and Design for Development*, 1993, p 198–209
20. N.S.M. El-Tayeb, K.O. Low, and P.V. Brevem, Enhancement of Surface Quality and Tribological Properties Using Ball Burnishing Process, *Mach. Sci. Technol.*, 2008, **12**, p 234–248.
21. D.G. Bansal, O.L. Eryilmaz, and P.J. Blau, Surface Engineering to Improve the Durability and Lubricity of Ti-6Al-4V Alloy, *Wear*, 2011, **271**, p 2006–2015.
22. C. Ohkubo, I. Shimura, T. Aoki, S. Hanatani, T. Hosoi, T. Okabe, In Vitro Wear Assessment of Titanium Alloy Teeth, *Proceedings of the International Tribology Conference, Nagasaki 2000*, p 1479–1483
23. X.X. Li, Y. Zhou, X.L. Ji, Y.X. Li, and S.Q. Wang, Effects of Sliding Velocity on Tribo-oxides and Wear Behavior of Ti-6Al-4V Alloy, *Tribol. Int.*, 2015, **91**, p 228–234. <https://doi.org/10.1016/j.triboint.2015.02.009>
24. R. Sahoo, S. Mantry, T.K. Sahoo, S. Mishra, and B.B. Jha, Effect of Microstructural Variation on Erosion Wear Behavior of Ti-6Al-4V Alloy, *Tribol. Trans.*, 2013, **56**, p 555–560. <https://doi.org/10.1080/10402004.2013.767400>
25. S. Hadke, R.K. Khatirkar, S.K. Shekhawat, S. Jain, and S.G. Sapate, Microstructure Evolution and Abrasive Wear Behavior of Ti-6Al-4V Alloy, *J. Mater. Eng. Perform.*, 2015, **24**, p 3969–3981. <https://doi.org/10.1007/s11665-015-1667-y>
26. H. Warlimont, Titanium and Titanium Alloys, 2018. https://doi.org/10.1007/978-3-319-69743-7_7
27. M.J. Donachie, *Titanium—A Technical Guide*, Vol 99 ASM International, 2000
28. S. Gollapudi, R. Sarkar, U. Chinta Babu, R. Sankarasubramanian, T.K. Nandy, and A.K. Gogia, Microstructure and Mechanical Properties of a Copper Containing Three Phase Titanium Alloy, *Mater. Sci. Eng. A*, 2011, **528**, p 6794–6803. <https://doi.org/10.1016/j.msea.2011.05.080>
29. Q.Y. Sun, Z.T. Yu, R.H. Zhu, and H.C. Gu, Mechanical Behavior and Deformation Mechanism of Ti-2.5Cu Alloy Reinforced by Nano Scale Precipitates at 293 and 77 K, *Mater. Sci. Eng. A*, 2004, **364**, p 159–165.
30. P. Mukhopadhyay, V. Singh, A. Bhattacharjee, and A.K. Gogia, Effect of Nano Ti₂Cu Precipitates in Ti6al4v2.5cu Alloy, *Mater. Today Proc.*, 2015, **2**, p 3580–3585.
31. J.C. Williams, R. Taggart, and D.H. Polonis, An Electron Microscopy Study of Modes of Intermetallic Precipitation in Ti-Cu Alloys, *Metal. Mater. Trans. B*, 1971, **2**, p 1139–1148.
32. S.C. Lim, M.F. Asbhy, and J.H. Brunton, Wear-Rate Transitions and Their Relationship to Wear Mechanisms, *Acta Metall.*, 1987, **35**, p 1343–1348.
33. N.P. Suh, An Overview of the Delamination Theory of Wear, *Wear*, 1977, **4**, p 1–6.
34. S. Jahanmir, N.P. Suh, and E.P. Abrahamson, Microscopic Observations of the Wear Sheet Formation by Delamination, *Wear*, 1974, **28**(2), p 235–249.
35. A. Molinari, G. Straffelini, B. Tesi, and T. Bacci, Dry Sliding Wear Mechanisms of the Ti6Al4V Alloy, *Wear*, 1997, **208**(1–2), p 105–112.

36. N.S.M. El-Tayeb, T.C. Yap, and P.V. Brevern, On the Tribo-cryogenic Characteristics of Titanium Alloys, *J. Eng. Tribol.*, 2010, **224**, p 395–409.
37. L. Yingjie, B. Xingui, and C. Keqiang, A Study on the Formation of Wear Debris during Abrasion, *Tribol. Int.*, 1985, **18**(2), p 107–111.
38. G. Straffelini and A. Molinari, Dry Sliding Wear of Ti-6Al-4V Alloy As Influenced by the Counterface and Sliding Conditions, *Wear*, 1999, **236**(1–2), p 328–338.

Publisher's Note Springer Nature remains neutral with regard to jurisdictional claims in published maps and institutional affiliations.

Springer Nature or its licensor (e.g. a society or other partner) holds exclusive rights to this article under a publishing agreement with the author(s) or other rightsholder(s); author self-archiving of the accepted manuscript version of this article is solely governed by the terms of such publishing agreement and applicable law.